Tip-Enhanced Raman Imaging of Photocatalytic Reactions on Thermally-Reshaped Gold and Gold-Palladium Microplates

SCHOLARONE™
Manuscripts

COMMUNICATION

Tip-Enhanced Raman Imaging of Photocatalytic Reactions on Thermally-Reshaped Gold and Gold-Palladium Microplates

Zhandong Li[a], Patrick Z. El-Khoury[b] and Dmitry Kurouski*[a,c]

Tip-enhanced Raman spectroscopy (TERS) was used to investigate plasmonic and photocatalytic properties of walled gold-palladium microplates (WAu@PdMPs), an alloy bimetallic nanostructures with unique chemical selectivity, and high sensitivity. We found that WAu@PdMPs can reduce 4-nitrobenzenethiol simultaneously to p,p'-dimercaptoazobisbenzene (DMAB) and 4-aminothiophenol, whereas such reduction yields only DMAB on the surface of monometallic nanostructures.

Introduction

Plasmonic bimetallic nanostructures have unique catalytic properties that arise from coupling of plasmonic and catalytic metal.[1-11] Noble metals in such nanostructures harvest solar radiation converting it into localized surface plasmons (LSPs), coherent oscillations of conductive electrons at the surface of plasmonic metals. Next, LSPs decay into hot electrons *via* direct interband, phonon-assisted intraband, and geometry-assisted transitions.[12-13] Hot electrons are short-living, highly energetic species[14,15] that are capable of driving chemical reactions in molecules located in the immediate vicinity to the metal surface.[16-19] Our group showed that core-shell gold-platinum nanoplates (Au@PtNPs) exhibit high selectivity in the photo-oxidation of 4-aminothiophenol (4-ATP).[20] Specifically, we observed a stepwise photo-oxidation of 4-ATP: first to 4-nitrobenzenethiol (4-NBT) then to *p,p'*-dimercaptoazobisbenzene (DMAB). Such selectivity was not observed using analogous monometallic structures, namely gold nanoplates (AuNPs). Core-shell gold-palladium microplates (Au@PdMPs),[21] on the opposite, demonstrated selectivity in photo-reduction, which was evident neither for their monometallic analogs (AuMPs) nor for core-shell Au@PtNPs.

From a perspective of nanostructure geometry, all bimetallic nanostructures can be divided into three classes: antenna-reactor, core-shell and alloy nanostructures.[22] While catalytic activity of the first two classes has been extensively investigated over the last decade, there is very little if anything is known about nanoscale plasmonic properties and corresponding photocatalytic properties of alloy bimetallic nanostructures.

Tip-enhanced Raman spectroscopy (TERS) is a powerful analytical tool that has single-molecule sensitivity and angstrom spatial resolution.[14-16] Under ambient laboratory conditions, TERS was employed to track chemical transformations at solid-air as well as solid-liquid interfaces.[23-26] Of relevance to this work are prior investigations by El-Khoury and co-workers, which were aimed at visualizing local optical fields on the surface of Ag nanowires (AgNWs) via TERS.[27] It was found that the recorded TERS maps trace the edges of Ag nanostructures, where local fields are optimally enhanced. Ren's group also explored the step-edge effects using sub-monolayer distributions of Pd on Au with TERS.[28] Phenyl isocyanide (PIC) was used as the molecular reporter, they have showed that in the spectra obtained on Pd step edges, the N≡C vibrational band of PIC was red-shifted by ~60 cm^{-1} compared with the molecules on Pd terrace. Those findings indicate that, at the step edges, the back donation from the d band of the metal to the antibonding π* orbital of PIC is greater than it at the terrace sites. This further support that molecules at Pd edges are more reactive compared with Pd atoms in terraces. These results together demonstrate that TERS is ideally suited for the visualization of nanoscale chemical transformations facilitated by mono- and bimetallic nanostructures.

In this work, we used TERS to investigate nanoscale plasmonic properties and photocatalytic properties of alloy Au@Pd bimetallic nanostructures. We found that AuMPs could be thermally reshaped into walled gold microplates (WAuMPs).[29] The appearance of walls is caused by a migration of Au atoms from the center of the microplate towards its edges. This process directly depends on the temperature and the time of the reshaping process. Electrochemical studies showed that thermally reshaped WAuMPs

have higher efficiency for the electrocatalytic conversion of methanol compared to AuMPs at lower formal potential. Using analogous synthetic approach, we prepared alloy Au@Pd bimetallic walled nanostructures (WAu@PdMPs, see Scheme S1 and SEM in Fig. S1). Using 4-NBT as a molecular reporter, we investigate hot-carrier driven reduction on the surface of WAu@PdMPs and their monometallic analogs WAuMPs with nanometer spatial resolution. We find that WAu@PdMPs exhibit drastically different plasmonic properties than the monometallic counterparts, WAuMPs. Overall, we track catalytically active and inactive sites on the surfaces of WAu@PdMPs with nanoscale precision and reveal structures of photocatalytic products of 4-NBT reduction.

Results and discussion

As shown in SEM (Fig. S1) and AFM height profile (Fig. S2), WAu@PdMP is an alloy without Pd islands. TERS spectrum of 4-NBT exhibited three vibrational bands centered at 1081, 1339 and 1576 cm^{-1}. We found that on the surface of WAu@PdMPs, 4-NBT could be reduced to DMAB that features the vibrational band at 1147 cm^{-1} and a doublet bands at 1397 and 1441 cm^{-1}.[20,21] TERS imaging of WAu@PdMPs (Fig. 1a-d, Fig. S3) revealed random formation of trans-DMAB without clear localization of reduction sites at edges, corners or the center part of WAu@PdMPs (Fig. 1b-c). These findings can be confirmed by statistical analysis of spectra collected from the edges/corners and center of WAu@PdMPs (Fig. S4 and Table S1).

Thus, WAu@PdMPs exhibit completely different photocatalytic activity comparing to their core-shell analogues Au@PdMPs and Au@PtNPs that exhibited substantially higher plasmonic activity at their edges/corners. We also analysed efficiency of plasmon-driven reduction of 4-NBT to DMAB on monometallic analogues of WAu@PdMPs. We found that WAu@PdMPs exhibit much stronger photocatalytic activities comparing to WAuMPs based on the yield of DMAB observed on their surfaces (Table S2).

At the same time, we found that WAuMPs reduce 4-NBT exclusively to DMAB (Fig. S5, S6), whereas on WAu@PdMPs this reaction yields both DMAB and 4-ATP, Fig. 1, Fig. S3 and S7. One can attribute such selectivity to the nature of the catalytic metal present in WAu@PdMPs. Pd is an excellent hydrogenation catalyst that will further reduce 4-NBT to 4-ATP, whereas relatively weak reduction properties of Au lead to observation of exclusively DMAB on the surface of WAuMPs. It should be also noted that such yield of 4-ATP on the surface of WAu@PdMPs can be linked to the strength of the electric field on the surface of these bimetallic nanostructures. Previously, Tian and Ren proposed that the strength of the electric field determines the ratio between DMAB and 4-ATP[30,31] where higher ratio of DMAB can be catalysed to 4-ATP on higher electric field. Link group recently reported that bimetallic nanostructures damp local electric fields via interband transitions of Pd.[32] Such electric field damping is results from the close energy levels of d-bands and Fermi levels in Pd.[22] Meanwhile, there is no LSPR damping on monometallic nanostructures (AuMPs and WAuMPs). On the other hand, monometallic nanostructures can support hybrid particle-tip
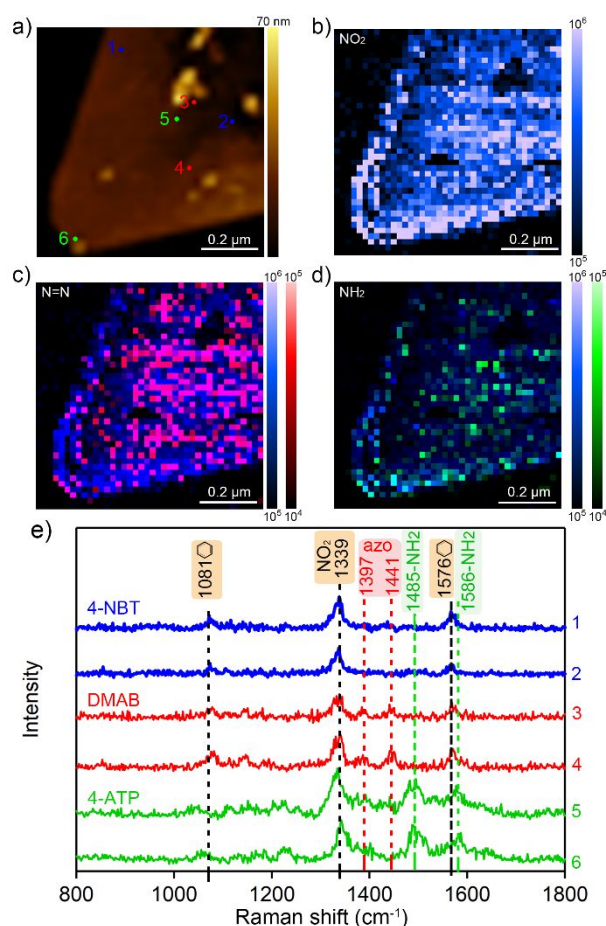

Fig. 1 (a) AFM image of WAu@PdMPs. (b) TERS image of NO$_2$ on WAu@PdMPs (20 nm per pixel). Overlapping TERS image of NO$_2$ vibration with (c) DMAB (d) 4-ATP vibration on WAu@PdMPs. Intensity of 1339 cm^{-1} band (NO$_2$) of 4-NBT is shown in blue, intensities of 1397 and 1441 cm^{-1} (azo) of DMAB is shown in red, intensities of 1485 cm^{-1} (NH$_2$) is shown in green. (e) Typical TERS spectra randomly picked up from chemical maps on (b-d) showing presence of 4-NBT (blue), DMAB (red) and NH$_2$ in green, which have been labeled in Fig. 1(a) and (e).

plasmonic modes that lead to extreme local field confinement and enhancement.[33]

Thus, one can expect that there are sites with high and low strengths of the electric field on the surface of WAu@PdMPs. High resolution TERS imaging showed that indeed very few 4-ATP sites overlap with sites at which DMAB is observed (Fig. S8). Alternatively, site-specific difference in formation of 4-ATP *vs* DMAB can be explained by far more complex interplay between Au and Pd in the structure of WAu@PdMPs. Elucidation of such an interplay will require extensive DFT calculations and direct measurements of electric field strength[34] of the surface of WAu@PdMPs, which are beyond the scope of the current work.

It should be noted that the observed TERS spectrum of 4-ATP has unexpectedly high intensity of 1485 vibration. Although this band is present in the vibrational spectrum of 4-ATP[35], it usually has very weak intensity in SERS/TERS. To investigate the origin of this phenomenon, we simulated molecular orientation-dependent Raman scattering from 4-ATP, see Fig. 2. Our results show that near-planar adsorption geometries of 4-ATP (~10-12

°) relative to the metal surface (xy plane in the inset of Fig. 2) provide the strongest relative intensity of the 1485 cm^{-1} mode. In other words, reaction products appear nearly planar atop Pd.
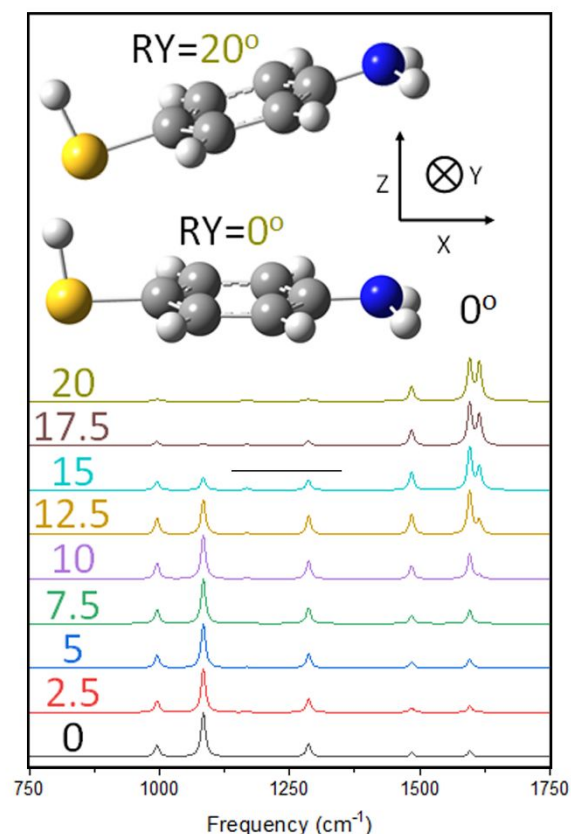
Fig. 2 Raman scattering from 4-ATP as a function of rotation around the Y-axis in the laboratory frame. Both the frame and the original and final orientation are shown in the upper parts of this Figure. Note that the metal surface is in the XY plane such that null rotation represents a planar adsorption geometry.
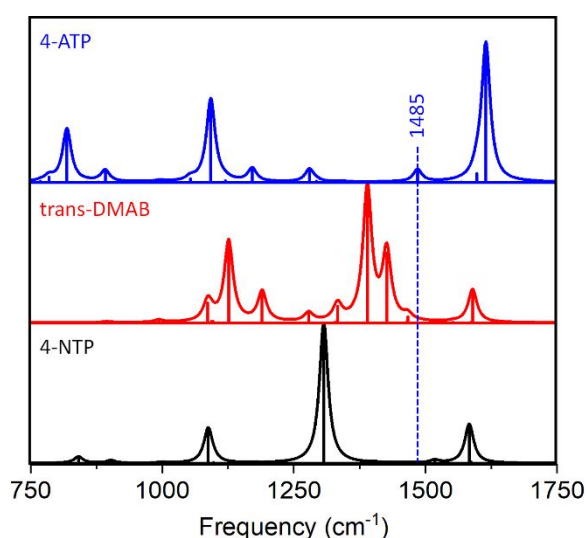

Fig. 3 Raman spectra (pbe/def2-TZVP) of 4-NBT, 4-ATP, and trans-DMAB. The vertical line that transects all spectra denotes 1485 cm^{-1}.

We finally note that according to our DFT calculations, an intense ~1485 cm^{-1} mode can be predicted for cis-DMAB, Fig. S9. A direct comparison of our experimental and calculated spectra nonetheless suggests that the formation of 4-ATP rather than cis-DMAB is more likely to occur on Pd based on our theoretical analysis. Specifically, the vibrational band at ~1575 cm^{-1} appears to red-shift in the experimental spectra (to 1586 cm^{-1}), as is the case of 4-ATP (Fig. 1, Fig. 3) and not cis-DMAB, where a blue-shift would be expected.

One can expect that trans-DMAB can be converted to cis-DMAB on the surface of WAu@PdMPs.[36,37] However, such isomerization of trans- to cis- DMAB requires near-UV light (313-436 nm) that was not used in our experiments. Using molecular dynamic calculations, Turanský and ci-workers proposed that trans-cis isomerization of DMAB can be induced by opto-mechanical as well as purely mechanochemical forces if squeezed between two metal clusters.[38] Although such squeezing cannot be fully excluded in our TERS experiments, highly unlikely such a strong mechanical force can be applied on DMAB using tapping mode TERS. Lastly, lack of a tunneling current used upon TERS imaging (AFM-TERS was used) suggest that unlikely trans-DMAB can be converted to cis-DMAB on the surface of WAu@PdMPs.[39]

Although WAuMPs exhibit higher electrocatalytic activity compared to AuMPs, they showed much lower photocatalytic activity compared to unmodified monometallic microplates. Specifically, much lower yields of DMAB on WAuMPs have been observed not only compared to WAu@PdMPs (Fig. 4), but also relative to AuMPs (Fig. S6, S10). This could be attributed to heat-induced melting of Au (111) crystal facets on their surface, which was present in AuMPs.[29] These results further demonstrate the importance of crystal structures on Au nanostructures in their catalytic activity.
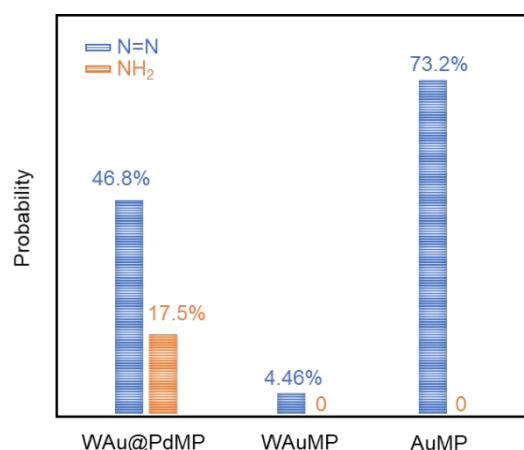
Fig. 4 Catalytic probability of AuMPs, WAuMPs, and WAu@PdMPs. The catalytic probability on these microplates was obtained by counting catalytic spots number of azo (blue bar) and amino (yellow bar) in the TERS maps and calculating the azo or amino occurrence ratio in all the catalytic events.

Conclusions

Using TERS, we have investigated plasmonic and photocatalytic properties of thermally-reshaped WAu@PdMPs, along with their monometallic analogs WAuMPs and AuMPs. We found that 4-NBT can be reduced to both DMAB and 4-ATP on these bimetallic WAu@PdMPs. However, on WAuMPs and AuMPs, only DMAB can be found resulting from the reduction of 4-NBT. The efficiency of these photo catalyzation are strongly associated with the nanoscale structure of these microplates. Our results also show that TERS imaging helps building up the bridge correlating the nanoscale structural and their corresponding catalytic reactivity on bimetallic nanostructures. Overall, our results should aid in guiding the rational design of novel bimetallic structures.

## Conflicts of interest

There are no conflicts to declare.

Acknowledgements

Notes and references

1   G. L. Brett, Q. He, C. Hammond, P. J. Miedziak, N. Dimitratos, M. Sankar, A. A. Herzing, M. Conte, J. A. Lopez-Sanchez, C. Kiely, D. Knight, S. Taylor, G. J. Hutchings, *Angew. Chem. Int. Ed.* 2011, **50,** 10136-10139.
2   F. Ksar, L. Ramos, B. Keita, L. Nadjo, P. Beaunier, H. Remita, *Chem. Mater.* 2009, **21,** 3677-3683.
3   M. Schrinner, S. Proch, Y. Mei, R. Kempe, N. Miyajima, M. Ballauff, *Adv. Mater.* 2008, **20,** 1928-1933.
4   N. Liu, M. L. Tang, M. Hentschel, H. Giessen, A. P. Alivisatos, *Nat. Mater.* 2011, **10,** 631-636.
5   C. Y. Chiu, M. H. Huang, *Angew. Chem. Int. Ed.* 2013, **52,** 12709-12713.
6   K. Gilroy, A. Sundar, M. Hajfathalian, A. Yaghoubzade, T. Tan, D. Sil, E. Borguet, R. Hughes, S. Neretina, *Nanoscale* 2015, **7,** 6827-6835.
7   A. S. Chauvin, S. Comby, B. Song, C. D. Vandevyver, J. C. G. Bünzli, *Chem. Eur. J.* 2008, **14,** 1726-1739.
8   L. Tong, C. M. Cobley, J. Chen, Y. Xia, J. X. Cheng, *Angew. Chem. Int. Ed.* 2010, **49,** 3485-3488.
9   J. C. G. Bünzli, A. S. Chauvin, C. D. Vandevyver, S. Bo, S. Comby, *Ann N.Y. Acad Sci* 2008, **1130,** 97-105.
10   Y. Zhao, C. Ye, W. Liu, R. Chen, X. Jiang, *Angew. Chem. Int. Ed.* 2014, **53,** 8127-8131.
11   P. Rameshkumar, S. Saranya, K. Sujatha, R. Ramaraj, *RSC adv.* 2015, **5,** 5038-5045.
12   F. Wang, C. Li, H. Chen, R. Jiang, L. D. Sun, Q. Li, J. Wang, J. C. Yu, C. H. Yan, *J. Am. Chem. Soc.* 2013, **135,** 5588-5601.

13   Z. Lou, M. Fujitsuka, T. Majima, *ACS Nano* 2016, **10,** 6299-6305.
14   M. D. Sonntag, J. M. Klingsporn, L. Garibay, D. Roberts, J. A. Dieringer, K. A. Scheidt, L. Jensen, G. C. Schatz, T. Seideman, R. P. Van Duyne, *J Phys Chem C* 2012, **116,** 478-483.
15   R. Zhang, Y. Zhang, Z. C. Dong, S. Jiang, C. Zhang, L. G. Chen, L. Zhang, Y. Liao, J. Aizpurua, Y. Luo, J. L. Yang, J. G. Hou, *Nature* 2013, **498,** 82-86.
16   D. Kurouski, *Vibr Spectrosc* 2017, **9,** 3-15.
17   D. Kurouski, M. Mattei and R. P. Van Duyne *Nano lett,* 2015, **15,** 7956-7962.
18   S. F. Becker, M. Esmann, K. Yoo, P. Gross, R. Vogelgesang, N. Park and C. Lienau, *ACS Photonics* 2016, **3,** 223-232.
19   J. Lee, K. T. Crampton, N. Tallarida and V. A. Apkarian, *Nature* 2019, **568,** 78-82.
20   Z. Li, D. Kurouski, J Phys Chem C 2020, 124, 12850-12854.
21   Z. Li, R. Wang, and D. Kurouski, *J Phys Chem Lett* 2020, **11,** 5531-5537.
22   K. Sytwu, M. Vadai, J. A. Dionne, *Advances in Physics: X* 2019, **4,** 394-418.
23   A. Bhattarai, P. Z. El-Khoury, *J Phys Chem Lett* 2019, **10,** 2817-2822.
24   J.-J. Sun, H.-S. Su, H.-L. Yue, S.-C. Huang, T.-X. Huang, S. Hu, M. M. Sartin, J. Cheng, B. Ren, *J Phys Chem Lett* 2019, **10,** 2306-2312.
25   N. Kumar, B. Stephanidis, R. Zenobi, A. J. Wain, D. Roy, *Nanoscale* 2015, **7,** 7133-7137.
26   E. M. van Schrojenstein Lantman, T. Deckert-Gaudig, A. J. Mank, V. Deckert, B. M. Weckhuysen, *Nat. Nanotechnol.* 2012, **7,** 583-586.
27   A. Bhattarai, K. T. Crampton, A. G. Joly, L. Kovarik, W. P. Hess, P. Z. El-Khoury, *J Phys Chem Lett* 2018, **9,** 7105-7109.
28   J. H. Zhong, X. Jin, L. Meng, X. Wang, H. S. Su, Z. L. Yang, C. T. Williams, B. Ren, *Nat Nanotechnol* 2017, **12,** 132-136.
29   R. Wang, D. Kurouski, *ACS Appl Mater Interfaces* 2019, **11,** 41813-41820.
30   Y. F; Huang, D. Y. Wu, H. P. Zhu, L. B. Zhao, G. K. Liu, B. Ren, Z. Q. Tian, *Phys. Chem. Chem. Phys.* 2012, **14,** 8485-8497.
31   Y. F. Huang, H. P. Zhu, G. K. Liu, D. Y. Wu, B. Ren, Z. Q. Tian, *J. Am. Chem. Soc.* 2010, **132,** 9244-9246.
32   A. Joplin, S. A. Hosseini Jebeli, E. Sung, N. Diemler, P. J. Straney, M. Yorulmaz, W. S. Chang, J. E. Millstone, S. Link, *ACS Nano* 2017, **11,** 12346-12357.
33   R. Wang, Z. He, A. V. Sokolov, D. Kurouski, *J Phys Chem Lett* 2020, **11,** 3815-3820.
34   J. M. Marr, Z. D. Schultz, *J. Phys. Chem. Lett.* 2013, **4,** 3268–3272.
35   J. Huang, Y. Zhu, M. Lin, Q. Wang, L. Zhao, Y. Yang, K. X. Yao, Y. Han, *J. Am. Chem. Soc.* 2013; **135,** 8552-8661.
36   Y. Yang, F. Teng, L. Yu, Y. Liu, P. Song, L. Xia, *ACS Omega* 2019, **4,** 7076-7081.
37   H. M. Bandara, S. C. Burdette, *Chem. Soc. Rev.* 2012, **41,** 1809-1825.
38   R. Turansky, M. Konopka, N. L. Doltsinis, I. Stich, D. Marx, *Phys. Chem. Chem. Phys.* 2010, **12,** 13922-13932.
39   J. Henzl, M. Mehlhorn, H. Gawronski, K. H. Rieder, K. Morgenstern, *Angew. Chem. Int. Ed.* 2006, **45,** 603-606.

TOC:
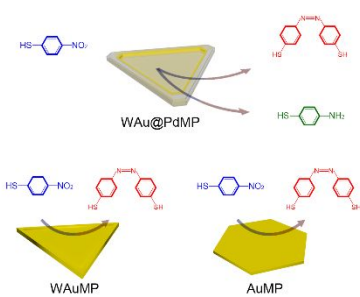
The plasmonic/photocatalytic properties of thermally-reshaped walled gold-palladium microplates (WAu@PdMPs) have been explored by TERS.